applied sciences

MDPI

Article

Data-Driven Damage Classification Using Guided Waves in Pipe Structures

Xin Zhang [1,2], Wensong Zhou [2,3,*], Hui Li [2,3] and Yuxiang Zhang [4]

1 Northwest Institute of Nuclear Technology, Xi'an 710024, China
2 Key Lab of Smart Prevention and Mitigation of Civil Engineering Disasters of the Ministry of Industry and Information Technology, Harbin Institute of Technology, Harbin 150090, China
3 Key Lab of Structures Dynamic Behavior and Control of the Ministry of Education, Harbin Institute of Technology, Harbin 150090, China
4 Xi'an Research Institute of Hi-Tech, Xi'an 710025, China
* Correspondence: zhouwensong@hit.edu.cn

Abstract: Damage types are important for structural condition assessment, however, for conventionally guided wave-based inspections, the characteristics extracted from the guided wave packets are usually used to detect, locate and quantify the damages, but not classify them. In this work, the data-driven method is proposed to classify the common damages in the pipe utilizing the guided wave signals obtained from numerous damage detection tests. The fundamental torsional mode T(0,1) is selected to conduct the guided wave-based damage detection to reduce the complexity of signal processing for its almost non-dispersive property. A total of 520 groups of experimental data under different degrees of damage were obtained to verify the proposed method. Finally, with help of a deep neural network (DNN) algorithm, all response data from the damages in the pipes were all clearly classified with quite high probability.

Keywords: pipe; guided wave; torsional mode; damage classification; MLP

Citation: Zhang, X.; Zhou, W.; Li, H.; Zhang, Y. Data-Driven Damage Classification Using Guided Waves in Pipe Structures. *Appl. Sci.* **2022**, *12*, 10874. https://doi.org/10.3390/app122110874

Academic Editors: Hossein Bisheh, Nan Wu and Yen-Fang Su

Received: 24 September 2022
Accepted: 24 October 2022
Published: 26 October 2022

1. Introduction

Pipelines play an increasingly important role in modern industries for the supply and distribution of required materials, such as natural gas, crude oil, steam, and hot water. They usually have a long operating life of more than 50 years, meanwhile, they are easy to suffer from aging defects and a wide variety of damages, which might result in terrible accidents. Therefore, damage detection for pipelines has become increasingly necessary. The damages in pipes usually include corrosion, seam weld cracks, stress rupture, material flaws, large deformation, and externally induced damage by a third party, etc. Usually, different damages lead to different influences and results, therefore, they are treated very differently.

Current pipe inspection methods include traditional ground-penetrating radar for buried pipelines [1,2], new but not proven pipeline robotics [3], etc. In comparison, strain measurement [4,5] and guided wave-based methods are more commonly used [6–10]. However, the former requires installing sensors for the entire length of the pipe in advance, which is not feasible in many practical situations. The latter has been proven to be effective and promising for damage detection in pipes over a long distance, even if the pipeline is buried. It can cover a large range of pipes from only a single inspection point. Moreover, guided wave-based methods recognize damages through the reflection or the transmission wave signals, which contain more information about the type, location, and degree of damage. They are extracted by a variety of signal processing methods, such as fast Fourier transform, continuous wavelet transform [11], singular value decomposition [12], principal component analysis [13], and machine learning [14,15]. For these traditional damage detection methods, structural damage is usually assumed to be the ideal shape, but no further differentiation is made. Therefore, damage classification is necessary for structural assessment.

In general, the damage type is related to its shape, which can be reconstructed through the interaction of guided wave with damages. Kim and Park [16] presented a quantitative study of the interaction of the T(0,1) torsional mode with axial and oblique defects in a pipe employing reflection signals from the defects and the mode decomposition technique. Muller et al. [17] used a circular network of piezoelectric disc transducers collect guided wave signals and reconstructed damage images with the total focusing method. The results indicate that crack- and hole-type of damages can be differentiated using geometric circularity and eccentricity shape factors. Da et al. [18] presented an analytical approach to reconstruct axisymmetric defects in pipelines using the torsional guided wave T(0, 1). This approach employed the reflection coefficients of the guided wave T(0, 1) scattered by different sizes of axisymmetric defects, and performed the reconstruction of defects by the inverse Fourier transform. Zimmermann et al. [19] used the guided wave tomography technique to map the corrosion thickness by transmitting guided waves. Zima [20] realized the size and shape estimation by only three sensors through the reconstruction of the shape of the reflected wavefront. Wu et al. [21] developed a damage shape recognition algorithm, which can capture the damage shape by describing the coordinates of the reflection point from the transducers to the damage edge. The above studies indicate that damage differentiation mainly depends on a complicated transducer array or reconstruction algorithm, which are difficult to carry out in the practical inspections.

A data-driven approach, by contrast, can overcome the difficulties of the complicated mathematical-physical model involved in wave propagations [22]. Borate et al. [23] proposed a data-driven approach to conduct damage detection using guided wave responses. The high-fidelity finite element method was used to establish a comprehensive database, and a neural network-based surrogate model was developed to relate the damage status with key features from these responses. The results indicate that the proposed approach could lead to an efficient damage detection. The data-driven model was also useful to predict waveform instead of the analytical model [22]. Moreover, data-driven methods based on deep neural networks (DNNs) show great ability for damage classification, because of the powerful data computing and analysis capability reported in recent research. Therefore, DNN is employed in this work for damage classification using guided wave signals.

In the following part, the mode selection, excitation, and reception of ultrasonic guided wave (UGW) in the pipe are introduced first. Additionally, the damage types in a pipe and their interactions with UGW are then analyzed. In Section 4, the experimental procedures are all illustrated in detail. Then, the multilayer neural network is built to perform damage classification, in which the effects of the number of hidden layers, the activation function and the noise level are all analyzed, followed by discussions and conclusions.

2. Mode Selection, Excitation, and Reception of UGW in Pipe

In pipe structures, there are three kinds of modes along the axial direction, which are, respectively, the longitudinal modes L(0, n), the torsional modes T(0, n), and the flexural modes F(m, n), where m and n are integers greater than zero, and represent the circumferential order and the radial order. The longitudinal modes that simultaneously contain the axial and radial displacements can be analogous to the Lamb wave in the plate, and correspondingly, the torsional modes only containing the circumferential displacement are similar to the SH wave in plate-like structures.

Figure 1 shows the group velocity dispersion curves of an aluminum pipe with an outside diameter of 102 mm and a thickness of 1.5 mm. It can be seen that, multiple modes exist at any frequency point, and at least two modes exist in a low frequency range. As the frequency increases, more modes arise. In Figure 1, there are only the first three modes displayed. It can be seen that the difference in the velocity of modes in the same group becomes smaller as the frequency increases, thus resulting in difficult separation for different modes in a high-frequency range.

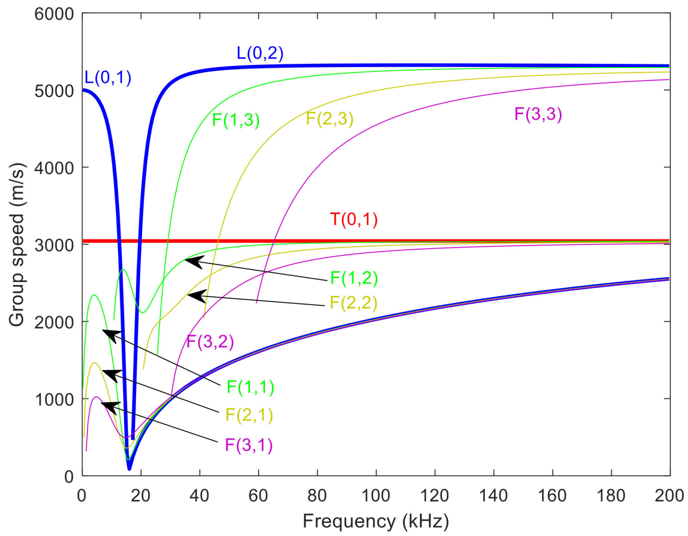

Figure 1. Group velocity dispersion curves of an aluminum pipe with an outside diameter of 102 mm.

From Figure 1, it is easily concluded that all the modes are more or less dispersive in any frequency range except the basic torsional mode T(0,1), which is quite appropriate for damage detection in the pipe because of the small waveform distortion. Moreover, the guided wave of the torsional mode only including shear strain $\varepsilon_{\theta z}$ and $\varepsilon_{r\theta}$ cannot propagate in fluid, which greatly reduces the energy dissipation to the internal medium. When the torsional mode is generated in pipe circumference uniformly, all the damage can be detected and, concurrently, the other flexural modes will be restrained to avoid overlapping between different modes.

Two methods, pitch-catch and pulse-echo, which take advantage of reflected and transmitted waves, respectively, are usually used to inspect structural status. For the former, the transmitted signals contain multiple unknown damage information and arrive simultaneously, therefore, it is difficult to determine the specific damage location. In this paper, the pulse-echo method is employed consequently. Moreover, the reflected signals from damage can be considered as an indicator to quantify the damage.

3. Damage Types in a Pipe and Their Interactions with UGW

Commonly, there exist a variety of damage types for a pipe after long service, which are, respectively, corrosion, dent, groove, hole, deposition, etc. Corrosion is the most common damage type resulting from interactions with the media inside and outside the pipe. There are several types such as pitting corrosion, uniform corrosion, corrosion under cover, sediment corrosion, etc. The dent is formed often because of third-party action such as the impact from excavators, weight extrusion, earthquakes, loose soil, etc. The groove is caused due to the development of minor damages left during the construction and manufacturing process or destruction by artificial factors. The hole is usually formed by severe corrosion and leads to media leakage. The deposition usually results in the thickening of the pipe wall, so it will not make a large difference to the waveform of the guided wave signal. Once the first four types of damages are present, there will be a significant safety problem. Therefore, in view of the above characteristics, the first four types of damages are investigated in this paper to realize damage classification.

When the guided wave interacts with damage, reflection, transmission, and diffraction signals are generated together, but in this work, only the reflected signals are analyzed. As mentioned previously, each type of damage has its unique characteristic for classification. Signals reflected from corrosion are usually longer in the time domain than signals from other conditions, because the pipe corrosion often takes up some length and area, leading to the reflected echoes overlapping each other. The third-party damage-like impact often forms a dent, where reflected signals contain more peaks than the original excitation signal, even if the detection signal is non-dispersive. The received wave packets are followed by some small wave peaks, which is mainly due to mode conversion in the front and rear edges of the impact position. The response signals from the groove and hole are usually regular and single, the amplitude of which is proportional to the damage size. Moreover, signals reflected from the pipe end are different from others not only in amplitude and frequency components, but also in the signal waveform.

Although these signal characteristics are different, as described, it is difficult to accurately classify the damage type using signal processing and quantitative analysis methods under real complex conditions. Taking advantage of a multi-layered perceptron, the more deep-seated characteristics can be automatically excavated, and the underlying sophisticated signal features can be easily learned to perform pattern recognition.

4. Experimental Investigations

4.1. Test Specimens and Setup

The specimens used in the experiment were a batch of thin aluminum pipes with dimensions of 102 mm × 1.5 mm (outside diameter × wall thickness). The damage was manufactured in a properly middle position along the axial direction. The guided wave transducer was a single magnetostrictive one. With the help of the signal generation and reception equipment (MsSRv5, SwRI, San Antonio, TX, US), the transducer can be used to excite and receive the guided wave signals with the time-sharing mode, thus realizing the pulse-echo mode, as shown in Figure 2.

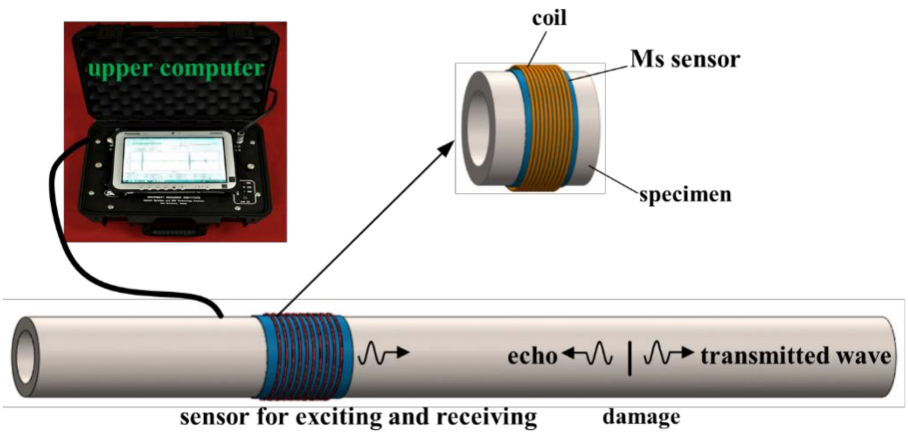

Figure 2. Damage detection setup based on a guided wave using a magnetostrictive sensor.

The excitation signal $f(t)$, defined as Equation (1), and its frequency spectrum are shown in Figure 3, in which it can be easily seen that the excitation is a sinusoidal tone-burst modulated by the Hanning window to restrain many side lobes at the center frequency of 128 kHz. If the signal frequency is high, the energy attenuation is excessively severe to detect for a long distance, and on the contrary, if the signal frequency is low, it is not sensitive to minor damage. In real application, the excitation signal was controlled by two channels to propagate mainly toward only one direction along the axial direction of the pipe, which can be explained by Equations (2) and (3):

$$f(t) = a[H(t) - H(t - n/f_c)][1 - \cos(2\pi f_c t/n)]\sin(2\pi f_c t) \quad (1)$$

where a is the amplitude coefficient and equal to 100 here; $H(\cdot)$ denotes the Heaviside step function; n is the cycle; and f_c denotes the center frequency of the exciting signal.

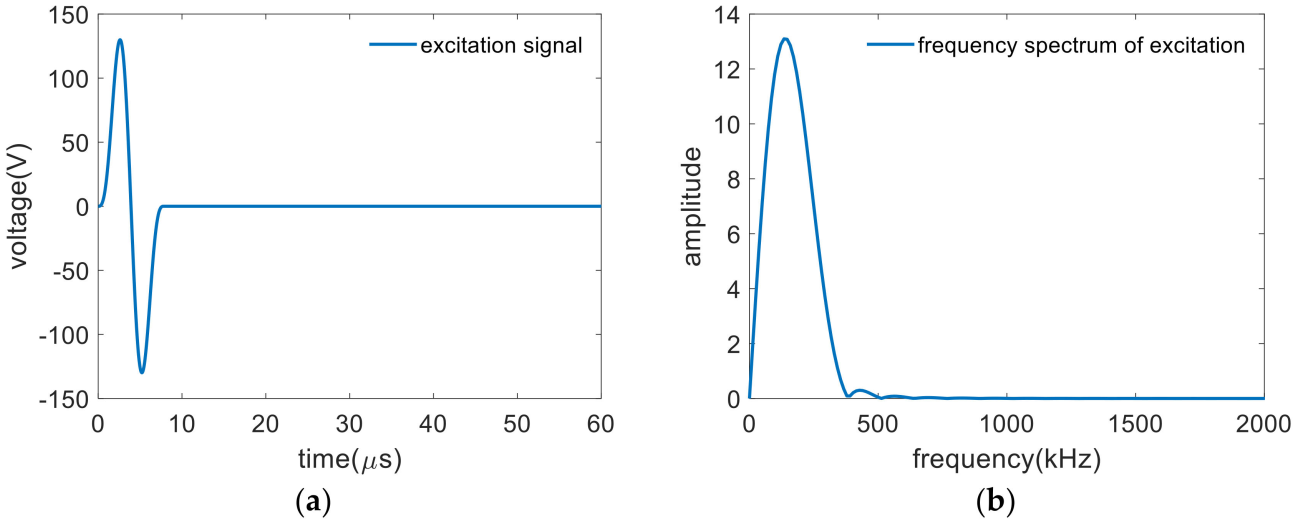

Figure 3. Excitation signal and its frequency spectrum: (**a**) excitation signal in time domain; and (**b**) frequency spectrum.

Suppose that two channels of transducers were fixed at a pipe, as shown in Figure 4, then signals in the left and right transducers can be expressed as s_1 and s_2, respectively.

$$\begin{cases} s_1 = A_1 \sin(\omega t + \varphi) \\ s_2 = A_2 \sin(\omega t + \varphi + \Delta\varphi) \end{cases}, \tag{2}$$

where $\omega = 2\pi f$ is the circular frequency; and $\Delta\varphi$ is the phase difference, which needed to be designed. In order to produce destructive interference in a certain direction, the amplitude must meet the condition of $A_1 = A_2 = A$. The signal propagating towards the right s_{right} and left s_{left} are as follows:

$$\begin{cases} s_{right} = s_1 + s'_2 = A\sin(\omega t + \varphi) + A\sin(\omega t + 2\pi\frac{d}{\lambda} + \varphi + \Delta\varphi) \\ s_{left} = s'_1 + s_2 = A\sin(\omega t + 2\pi\frac{d}{\lambda} + \varphi) + A\sin(\omega t + \varphi + \Delta\varphi) \end{cases} \tag{3}$$

where d is the distance of two transducers, and λ is the wavelength of the guided wave at the frequency f. If only the guided wave propagating towards the right is needed, Equation (4) can be obtained by solving Equation (3):

$$\begin{cases} d = [-2(k_1 + k_2) + 1]\frac{\lambda}{4} \\ \Delta\varphi = [2(k_2 - k_1) + 1]\frac{\pi}{2} \end{cases} \tag{4}$$

where k_1 and k_2 are both integers. For the simplest condition, $d = \lambda/4$, the phase difference $\Delta\varphi$ should be $\pi/2$.

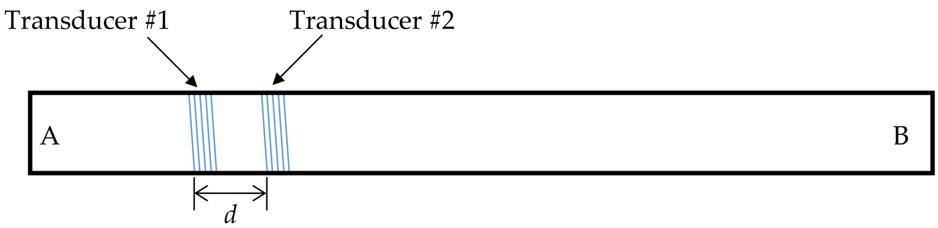

Figure 4. Sketch map of two channels of transducers in the pipe, where A and B stand for the different pipe ends.

4.2. Dataset Preparation of Guided Wave Signals

A total of 520 guided wave signals were obtained following the above process. All signals can be divided into five categories, as listed in Table 1. They were associated with five cases of no damage, corrosion, dent led by impact, groove and pipe end, respectively. To reduce the effect of measurement noise, the received signals were averaged over 50 repetitions of the experiment within 1 min.

Table 1. Damage types and number of signals.

Signal Type	Number	Typical Picture
No damage	70	
Corrosion	70	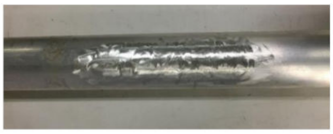
Dent led by impact	100	
Groove	80	
Pipe end	200	

Note: The yellow circle in the typical picture of groove stands for the groove position.

Ten signals for each type were plotted in Figure 5, in which the available signals were intercepted as 100 μs length from their original test signals at the sampling frequency of 1 MHz. For every damage type, the signals were obtained from different sizes of damage and different lengths of pipes to simulate as many damage states as possible. Furthermore, they were measured at different times of day, which means that the experiments were conducted under different environmental conditions. This increased the robustness of damage classification. Moreover, the signals were normalized within the full range; therefore, the amplitudes of intercepted signals were very different in Figure 5.

It can be seen from the time-domain signals of guided waves that the wave packets have very complicated characteristics under different damage types and degrees. The reason is the multiple mode conversions and interaction between guided waves and different damages, which increase the difficulty of signal interpretation. By using a single signal feature, it is difficult to distinguish the signals under different working conditions. Therefore, this paper uses the neural network to further process the signal. For conventional signal analysis, some features are usually extracted for further analysis, such as the amplitude and location of the peak in the time domain, the time-of-flight, the peak frequency, the average frequency, and other statistic features. While for the neural network, the input dataset is the original signals without processing, and the time-consuming is not seriously affected during network training and testing.

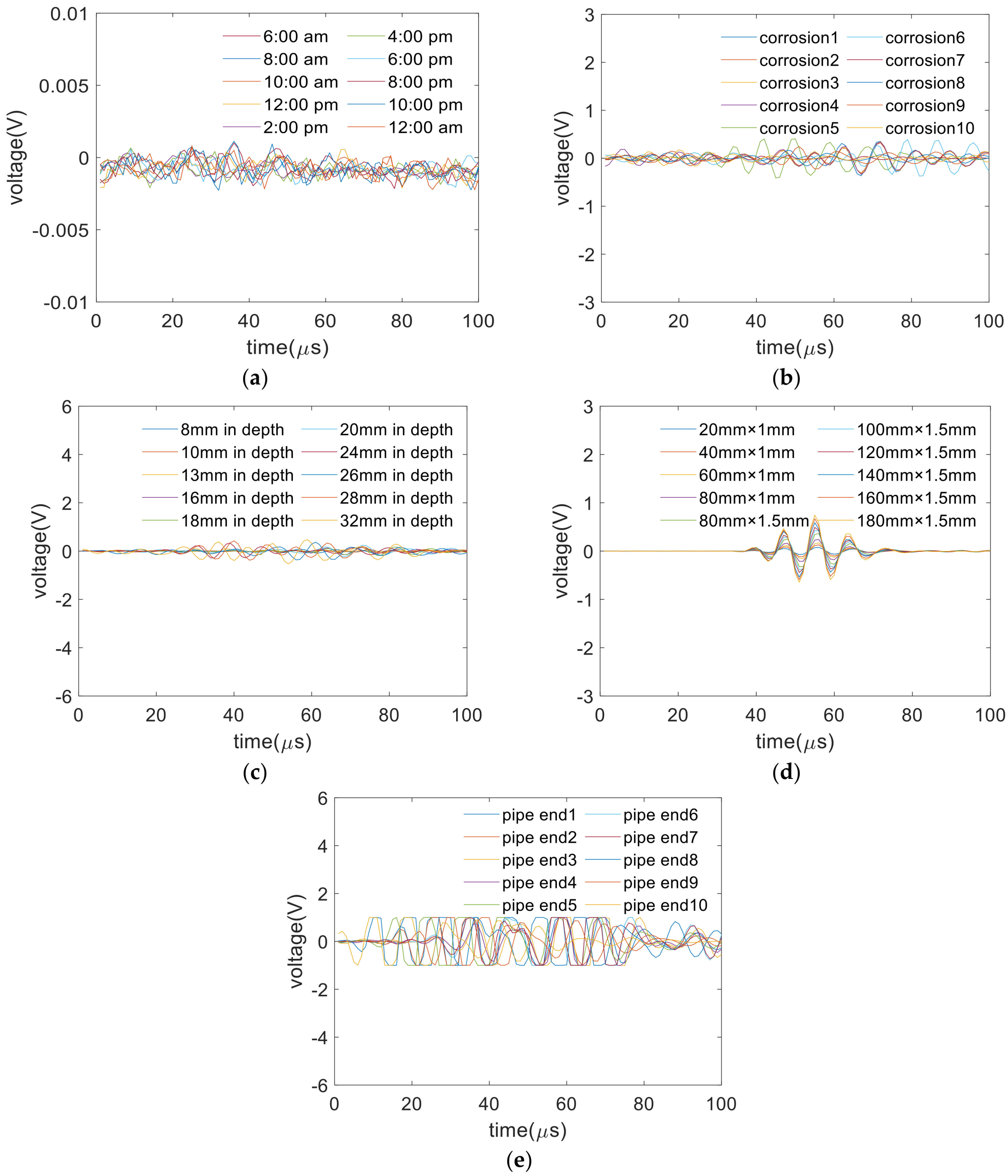

Figure 5. Typical reflected signals of the five types of damage: (**a**) echoes of no-damage; (**b**) echoes of corrosion; (**c**) echoes of dent; (**d**) echoes of groove; and (**e**) echoes of pipe end.

5. Training and Validation of the Neural Network

For data-driven damage classification, a multi-layer ANN framework was established. The neural network consisted of input, hidden, and output layers. In this section, the effect of the number of hidden layers was investigated first. Then, the activation function effect between tanh and ReLU was analyzed. Lastly, strong noise was considered to verify the robustness of MLP for damage classification.

5.1. The Number Effect of Hidden Layers

The sizes of the input, hidden, and output layers were set to 100, 20, and 5, respectively. The softmax function was selected as the classifier in the output layer, which is expressed in Equation (5). The activation function in the hidden layers is an all hyperbolic tangent sigmoid function tansig, i.e., tanh, which solved the zero-centered output problem in the sigmoid function. The expression and geometry image of tanh can be seen in Equation (6) and Figure 6, respectively. To investigate the effect of the hidden layers number, neural networks containing one and two hidden layers (called multi-layered perceptron, as shown in Figure 7) were built, respectively. The results are shown in Table 2.

$$\hat{y}_i = \frac{e^{a_i}}{\sum_{l=1}^{n} e^{a_l}},\ i \in [1, n] \tag{5}$$

where a_i denotes the value before the softmax classifier in the neural network, n = 5 means the category number, and $\hat{y}_i$ is the prediction probability belonging to the category i, in which the functional relation $\sum_{i=1}^{n} \hat{y}_i = 1$ must be met.

$$\tanh(x) = \frac{e^x - e^{-x}}{e^x + e^{-x}} \tanh(x) = \frac{e^x - e^{-x}}{e^x + e^{-x}} \tag{6}$$

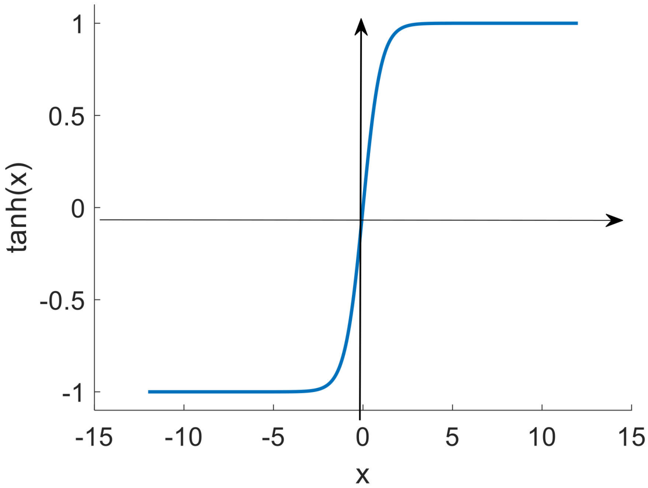

Figure 6. Hyperbolic tangent function tanh.

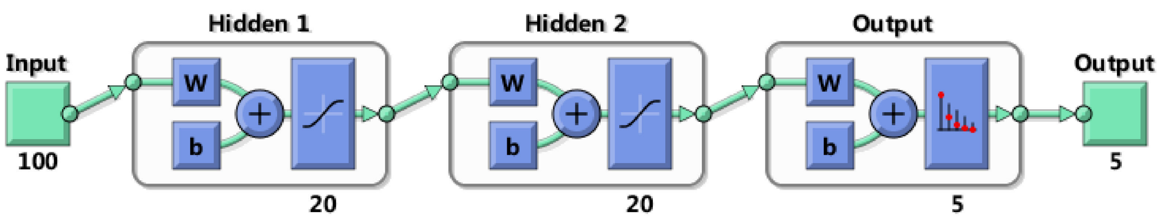

Figure 7. The neural network framework of MLP containing two hidden layers.

Table 2. Comparison of the number effect of hidden layers.

Hidden Layer Numbers	Iterations Epochs	Test Accuracy
1	20	88.5%
2	13	93.6%

From Table 2, it can be seen that the number of hidden layers severely affects the recognition accuracy, and a neural network with two hidden layers is more effective for processing guided-wave signals obtained from the pipe.

5.2. Activation Function Effect between Tanh and ReLU

Two frequency-used functions tanh and ReLU were compared in this work. The ReLU function shown in Equation (7) was simple, but it is an important achievement in recent years.

$$\mathrm{ReLU}(x) = \max(0, x) = \begin{cases} x \mathrm{if} x > 0 \\ 0 \mathrm{if} x \leq 0 \end{cases} \quad (7)$$

where max(·) refers to the larger value between two figures.

The neural networks framework plotted in Figure 8 were established with Python. The loss function was usually set as the cross entropy as Equation (8). The regularization term is always brought in to avoid overfitting, so correspondingly, the final loss function is expressed in Equation (9), which can reflect the difference between the real label and the prediction label. When the final loss function $L'(y_i, \hat{y}_i)$ is equal to zero, this means that the prediction label is completely identical to the real label. In addition, the batch gradient descent back propagation method is adopted to update the MLP parameters, considering that the sample set is not very large.

$$L(y_i, \hat{y}_i) = -\sum_{i=1}^{n} y_i \log(\hat{y}_i) \quad (8)$$

$$L'(y_i, \hat{y}_i) = L(y_i, \hat{y}_i) + \frac{\lambda}{2N} \sum_{j=1}^{N} w_j^2 \quad (9)$$

where y_i represents the real labels, and in this paper, the labels y_i = [1, 0, 0, 0, 0], [0, 1, 0, 0, 0], [0, 0, 1, 0, 0], [0, 0, 0, 1, 0], and [0, 0, 0, 0, 1] correspond to the experimental conditions of no damage, corrosion, dent, groove, and pipe end; λ is the regularization coefficient; and N is the number of all the parameters w_j.

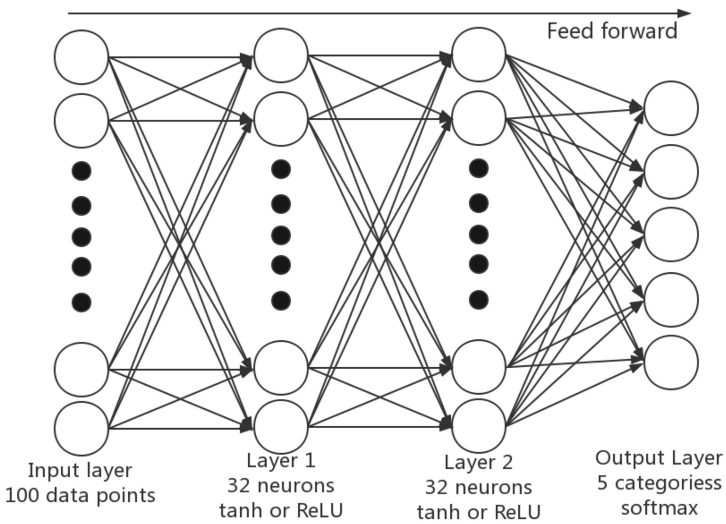

Figure 8. The multilayer feed-forward neural network framework.

In order to accurately identify the signal type, an MLP with two hidden layers containing 32 neurons in each layer was employed. The final loss function $L'(y_i, \hat{y}_i)$ of the training set was set to be below 5×10^{-3}; the learning rate was 3×10^{-3}; and the regularization coefficient λ in Equation (9) was set as 1×10^{-5}. After training with 420 samples randomly selected in the gross 520 signal samples, the test result of what remained was obtained. The corresponding training processes for the training set are shown in Figure 9, from which it can be seen that the training process of the network containing two ReLU hidden layers converged faster. The L′ of the neural network with tanh hidden layers dropped to 4.91 $\times 10^{-3}$ at 1244 epochs, and that with ReLU hidden layers dropped to 3.27×10^{-3} at 885 epochs. The training and test confusion matrices of these two kinds of multi-layer neural network are shown in Figures 10 and 11, respectively. It is easy to obtain the conclusion that the ReLU activation function is more effective for the pattern recognition of guided wave signals.

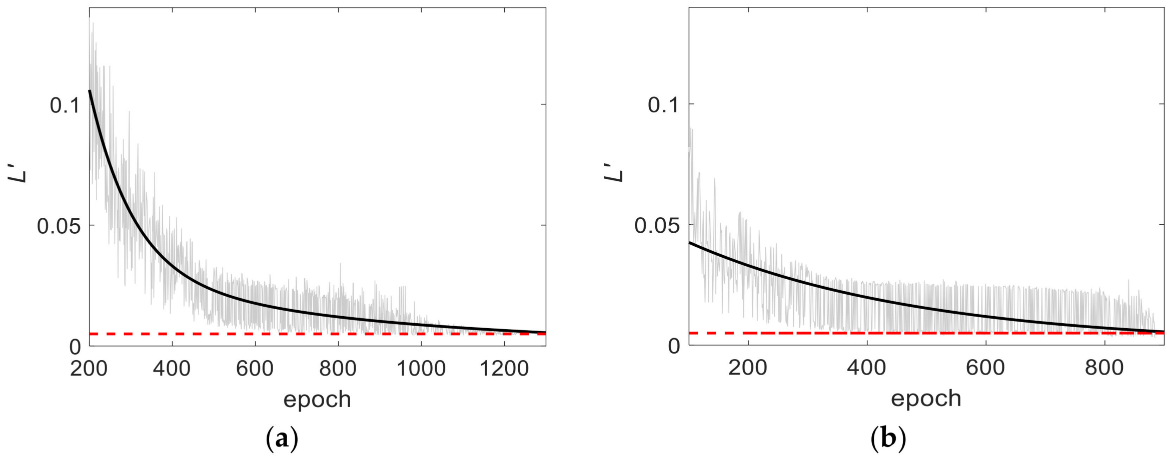

Figure 9. Training processes of the multi-layer neural network with different activation functions: (**a**) tanh; (**b**) ReLU.

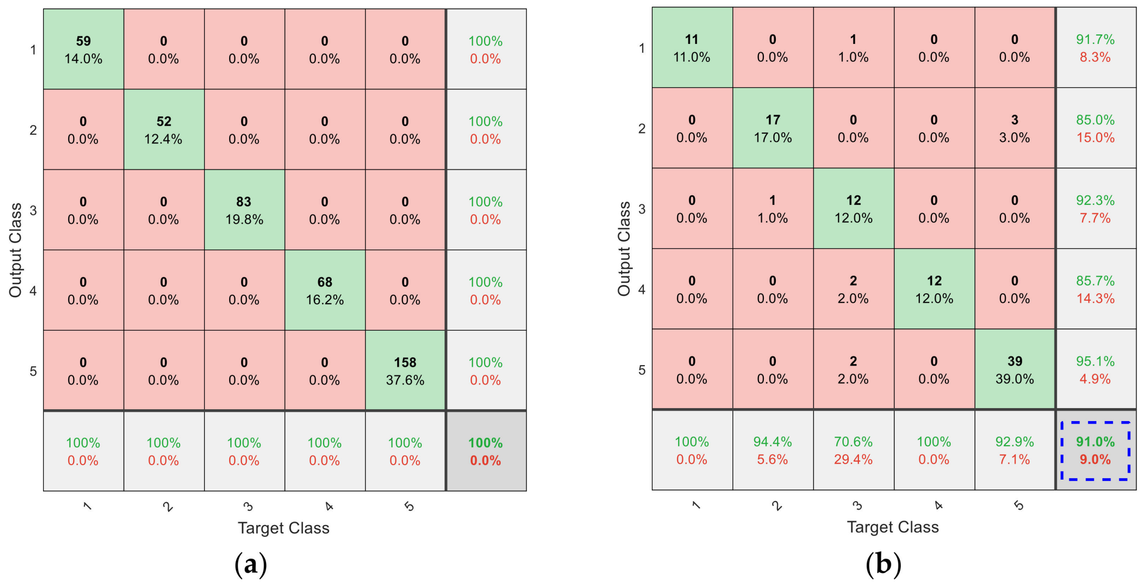

Figure 10. Training and test confusion matrices of neural network with tanh hidden layers: (**a**) training confusion matrix; and (**b**) test confusion matrix.

5.3. Noise Effect

For investigating the validity of the proposed method in the presence of noise, Gaussian noise was added to the guided wave signals with two different levels, SNR = 30 and 20 dB, respectively.

Then, signals were trained and tested by the multi-layer neural network with ReLU hidden layers, which shows good results of almost 100% during the training process for 420 signals with both 20 dB and 30 dB SNR noises, but the test results of 100 samples, i.e., the recognition accuracy is, respectively, 88% for signals with 30 dB SNR noise and 82% for signals with 20 dB SNR noise. These results were unable to meet the requirement in the structural health monitoring (SHM) field, so it can be concluded that it is necessary for guided waves to be filtered before pattern recognition. The test results of the signals with 30 dB and 20 dB SNR noise are displayed in Figure 12, which also shows that confusion is easily made among the labels 1, 2, and 3—that is to say, the signals from no damage, extensive corrosion, and dent led by impact.

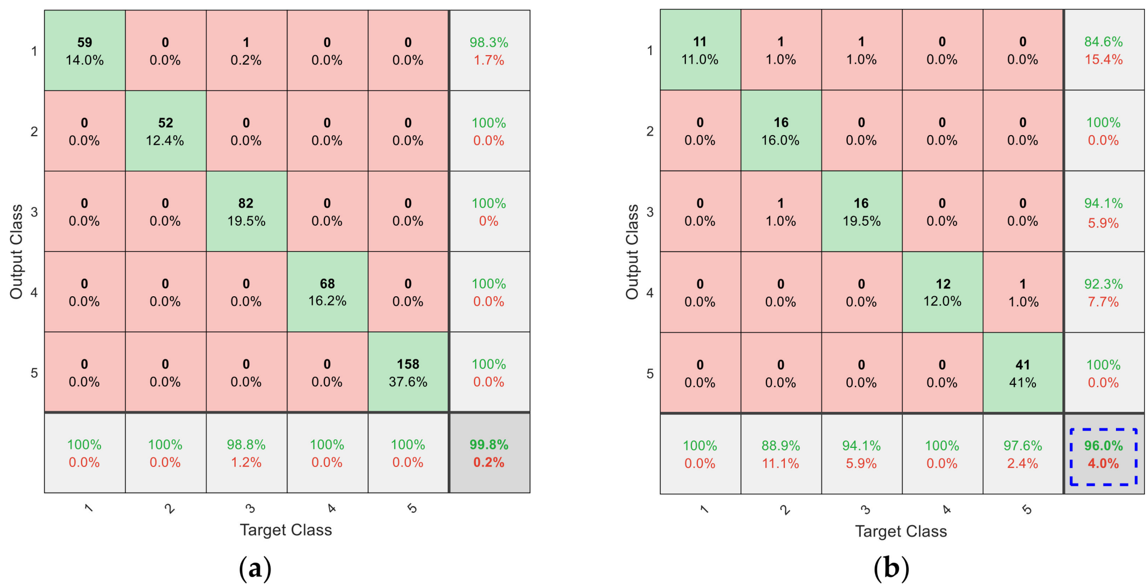

Figure 11. Training and test confusion matrices of neural network with ReLU hidden layers: (**a**) training confusion matrix; (**b**) test confusion matrix.

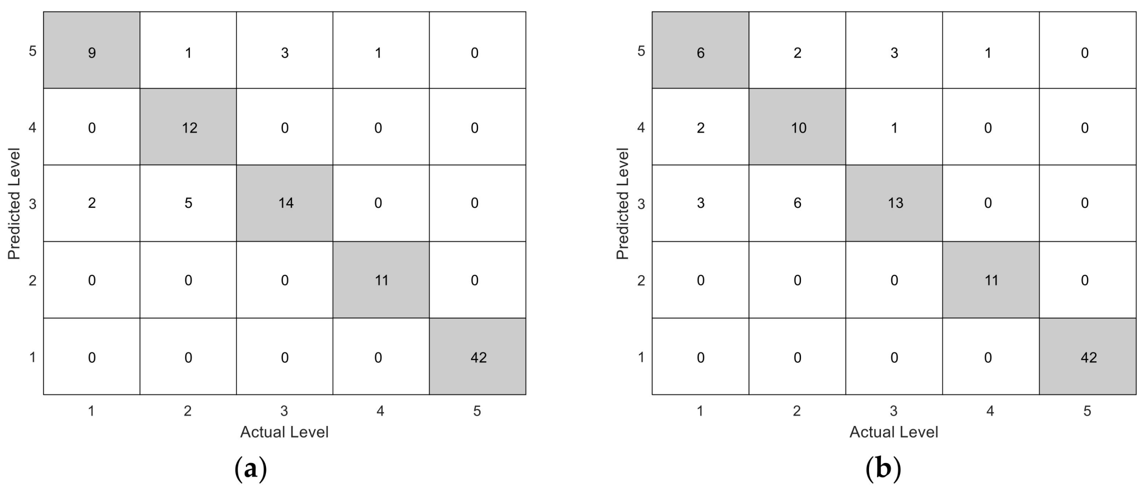

Figure 12. Test results under the effect of noise: (**a**) SNR = 30 dB; and (**b**) SNR = 20 dB.

6. Conclusions

Due to the complicated mathematical-physical model involved in wave propagations and interaction between guided wave and damages, it is difficult to identify the damage type through the conventional guided wave signal processing methods. In order to solve this problem, we proposed a data-driven method for the damage classification of pipeline structures using reflected guided wave signals. This method can distinguish damage types through the time-domain guided wave signals. The ability of the guided wave method is improved for SHM. The specific conclusions are as follows:

(1) For guided wave signal processing, the ANN framework with two hidden layers has higher classification efficiency and accuracy than the framework with only one layer. The results show that the number of hidden layers seriously affects the recognition accuracy. The neural network with two hidden layers can converge only after 13 iterations, reaching 94.6% classification accuracy. It is more effective for processing guided wave signals obtained from pipes.

(2) Using ReLU as the hidden layer activation function has a better classification effect. The recognition effects of two activation functions, tanh and ReLU, were compared on a

training set containing 420 sample data and a test set containing 100 sample data. The training process of the network with two ReLU hidden layers converges faster and is more accurate for damage type recognition.

(3) By adding Gaussian noise with the SNR of 30 dB and 20 dB to the original signals, the robustness to noise of the proposed method was investigated. The corresponding recognition accuracy was 88% and 82%, respectively. Therefore, guided wave signals with low SNR may lead to misjudgment, and filtering is necessary for the damage classification.

Author Contributions: Investigation, software, formal analysis, writing – original draft, X.Z.; supervision, writing-review & editing, funding acquisition, W.Z.; conceptualization, project administration, H.L.; resources, Y.Z. All authors have read and agreed to the published version of the manuscript.

Funding: The study was supported by the National Science Foundation of China (Grant Nos. 51978217, 51975581).

Institutional Review Board Statement: Not applicable.

Informed Consent Statement: Not applicable.

Data Availability Statement: Data available from the corresponding author upon reasonable request.

Conflicts of Interest: The authors declare no conflict of interest.

References

1. Crocco, L.; Prisco, G.; Soldovieri, F.; Cassidy, N.J. Early-stage leaking pipes GPR monitoring via microwave tomographic inversion. *J. Appl. Geophys.* **2009**, *67*, 270–277. [CrossRef]
2. Wahab, S.W.; Chapman, D.N.; Rogers, C.D.F.; Foo, K.Y.; Metje, N.; Nawawi, S.W.; Isa, M.N.; Madun, A. Assessing the condition of buried pipe using ground penetrating radar (GPR). *Int. Arch. Photogramm. Remote Sens. Spat. Inf. Sci. ISPRS Arch.* **2018**, *42*, 77–81. [CrossRef]
3. Kazeminasab, S.; Sadeghi, N.; Janfaza, V.; Razavi, M.; Ziyadidegan, S.; Banks, M.K. Localization, mapping, navigation, and inspection methods in in-pipe robots: A review. *IEEE Access* **2021**, *9*, 162035–162058. [CrossRef]
4. Lee, H.; Sohn, H. Damage detection for pipeline structures using optic-based active sensing. *Smart Struct. Syst.* **2012**, *9*, 461–472. [CrossRef]
5. Chmelko, V.; Garan, M.; Šulko, M. Strain measurement on pipelines for long-term monitoring of structural integrity. *Meas. J. Int. Meas. Confed.* **2020**, *163*, 107863. [CrossRef]
6. Guan, R.; Lu, Y.; Duan, W.; Wang, X. Guided waves for damage identification in pipeline structures: A review. *Struct. Control Health Monit.* **2017**, *24*, e2007. [CrossRef]
7. Bagheri, A.; Rizzo, P.; Li, K. Ultrasonic imaging algorithm for the health monitoring of pipes. *J. Civ. Struct. Health Monit.* **2017**, *7*, 99–121. [CrossRef]
8. Niu, X.; Duan, W.; Chen, H.-P.; Marques, H.R. Excitation and propagation of torsional T(0,1) mode for guided wave testing of pipeline integrity. *Meas. J. Int. Meas. Confed.* **2019**, *131*, 341–348. [CrossRef]
9. Miao, H.; Huan, Q.; Wang, Q.; Li, F. Excitation and reception of single torsional wave T(0,1) mode in pipes using face-shear d24 piezoelectric ring array. *Smart Mater. Struct.* **2017**, *26*, 025021. [CrossRef]
10. Zhang, H.; Du, Y.; Tang, J.; Kang, G.; Miao, H. Circumferential SH wave piezoelectric transducer system for monitoring corrosion-like defect in large-diameter pipes. *Sensors* **2020**, *20*, 460. [CrossRef]
11. Li, J.; Lu, Y.; Guan, R.; Qu, W. Guided waves for debonding identification in CFRP-reinforced concrete beams. *Constr. Build. Mater.* **2017**, *131*, 388–399. [CrossRef]
12. Tang, M.; Wu, X.; Cong, M.; Guo, K. A method based on SVD for detecting the defect using the magnetostrictive guided wave technique. *Mech. Syst. Signal Process.* **2016**, *70*, 601–612. [CrossRef]
13. Wang, P.; Zhou, W.; Bao, Y.; Li, H. Ice monitoring of a full-scale wind turbine blade using ultrasonic guided waves under varying temperature conditions. *Struct. Control Health Monit.* **2018**, *25*, e2138. [CrossRef]
14. Liu, H.; Zhang, Y. Deep learning based crack damage detection technique for thin plate structures using guided lamb wave signals. *Smart Mater. Struct.* **2020**, *29*, 015032. [CrossRef]
15. Li, Z.; Li, D.; Chen, Y. Deep learning-based guided wave method for semi-grouting sleeve detection. *J. Build. Eng.* **2022**, *46*, 103739. [CrossRef]
16. Kim, Y.-W.; Park, K.-J. The interaction of fundamental torsional guided waves from axial and oblique defects in pipes. *Insight: Non-Destr. Test. Cond. Monit.* **2021**, *63*, 334–340. [CrossRef]
17. Muller, A.; Soutis, C.; Gresil, M. Image reconstruction and characterisation of defects in a carbon fibre/epoxy composite monitored with guided waves. *Smart Mater. Struct.* **2019**, *28*, 065001. [CrossRef]
18. Da, Y.; Wang, B.; Liu, D.Z.; Qian, Z. An analytical approach to reconstruction of axisymmetric defects in pipelines using T(0, 1) guided waves. *Appl. Math. Mech. Engl. Ed.* **2020**, *41*, 1479–1492. [CrossRef]

19. Zimmermann, A.A.E.; Huthwaite, P.; Pavlakovic, B. High-resolution thickness maps of corrosion using SH1 guided wave tomography. *Proc. R. Soc. A Math. Phys. Eng. Sci.* **2021**, *477*, 20200380. [CrossRef]
20. Zima, B. Damage detection in plates based on Lamb wavefront shape reconstruction. *Measurement* **2021**, *177*, 109206. [CrossRef]
21. Wu, Y.; Shen, X.; Li, D. Numerical and experimental research on damage shape recognition of aluminum alloy plate based on Lamb wave. *J. Intell. Mater. Syst. Struct.* **2021**, *32*, 2273–2288. [CrossRef]
22. Silva, S. Data-driven model identification of guided wave propagation in composite structures. *J. Braz. Soc. Mech. Sci. Eng.* **2018**, *40*, 543. [CrossRef]
23. Borate, P.; Wang, G.; Wang, Y. Data-driven structural health monitoring approach using guided Lamb wave responses. *J. Aerosp. Eng.* **2020**, *33*, 04020033. [CrossRef]